PCCP

PAPER

View Article Online
View Journal

Cite this: DOI: 10.1039/d5cp04677g

NIR excitation-driven conformational isomerizations of thymol and carvacrol isolated in a nitrogen cryomatrix

Leonardo J. Duarte, *[abc] Cláudio M. Nunes, [c] Ataualpa A. C. Braga, [a] R. Fausto [cd] and A. J. Lopes Jesus *[e]

Thymol (2-isopropyl-5-methylphenol) and carvacrol (5-isopropyl-2-methylphenol) differ only in the relative positions of the hydroxyl and alkyl substituents, yet this subtle change reverses their torsional energy profiles: in thymol, isopropyl rotation is more hindered than OH torsion, whereas in carvacrol the opposite occurs. These features make the two compounds ideal model systems to investigate how differences in OH and isopropyl torsional barriers influence the redistribution of vibrational energy following near-infrared (NIR) excitation of the 2νOH overtone. Monomers of both compounds were isolated in a nitrogen matrix at 15 K and irradiated within the profile of the 2νOH overtone band (7110 to 7060 cm^{-1}) by using tunable laser light. Spectroscopic monitoring revealed selective and bidirectional interconversion between rotamers differing in the OH orientation. On the contrary, no interconversion between conformers differing in the isopropyl orientation was observed. This is particularly noteworthy for carvacrol, as its isopropyl torsional barrier is comparable in magnitude to that of the OH rotation. These findings support OH-rotamerization as the main route for vibrational energy redistribution, independent of the relative barrier heights. The photogenerated higher-energy *cis*-OH rotamers were observed to relax spontaneously to their *trans* counterparts *via* intramolecular hydrogen-atom tunneling, whose kinetics were quantitatively determined.

Received 1st December 2025,
Accepted 17th April 2026

DOI: 10.1039/d5cp04677g

rsc.li/pccp

1. Introduction

Since the groundbreaking work of Pettersson, Lundell, Khriachtchev and Räsänen in the late 1990s, which demonstrated the narrowband Near Infrared (NIR) induced rotamerization of formic acid under matrix-isolation conditions,[1] the combination of NIR laser sources with the matrix-isolation technique has emerged as a powerful tool for triggering, in a very selective way, conformational transformations in a wide variety of molecules. Carboxylic acids have been extensively studied systems,[2–18] though many other types of molecules have also been examined. These include the Kojic[19] and squaric[20] acids, aminoacids,[21–24] nucleobases and their derivatives,[25–27] phenol and indole derivatives,[28–31] among other species.[32–36] Comprehensive reviews have also been published, highlighting key achievements and advances in the field.[37–41]

Vibrationally-induced conformational transformations are fundamentally controlled by Intramolecular Vibrational Energy Redistribution (IVR),[42–46] wherein relaxation following excitation of, for example, OH, CH, NH, or NH_2 stretching vibrations, or their combinations and overtones, leads to a transfer of energy to a reactive torsional coordinate, resulting in the conformational change. For rotamerization to occur under NIR excitation, the deposited vibrational energy should typically exceed the torsional barrier. However, IVR can sometimes promote conformational changes even when the initially excited vibrational mode lies below this threshold.[47] The mechanism behind this process is still a matter of debate in the literature. Based on the experimentally observed isomerization of formic acid triggered by the excitation of normal modes below the barrier, Pettersson *et al.* proposed that the mechanism must involve tunneling effects.[47] In a recent theoretical study from our laboratory on HONO isomerization, we found a similar mechanism, suggesting that IR-induced isomerization below the barrier may occur *via* tunneling assisted IVR.[48]

[a] *Department of Fundamental Chemistry, Institute of Chemistry, University of São Paulo, 05508-900, São Paulo, Brazil. E-mail: ljduarte@iq.usp.br*
[b] *Center for Natural and Human Sciences, Federal University of ABC, 09280-560, Santo André, SP, Brazil*
[c] *University of Coimbra, CQC-IMS, Department of Chemistry, 3004-535, Coimbra, Portugal*
[d] *Department of Physics, Spectroscopy@IKU, Faculty Sciences and Letters, Istanbul Kultur University, Bakirkoy, Istanbul 34158, Turkey*
[e] *CQC-IMS, Faculty of Pharmacy, University of Coimbra, 3004-295, Coimbra, Portugal. E-mail: ajorge@ff.uc.pt*

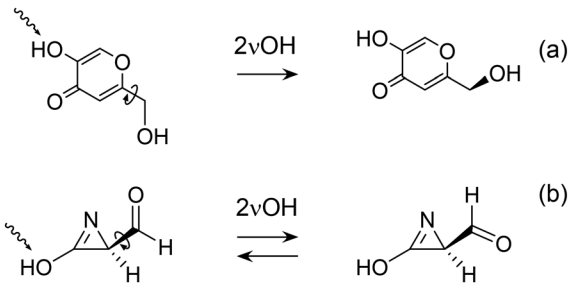

Fig. 1 Illustrative examples of rotamerization of heavy-atom fragments triggered by NIR excitation of 2νOH overtones of (a) kojic acid and (b) 3-hydroxy-2-formyl-azirine.

For OH-containing molecules, excitation of the first overtone of an OH stretching mode (2νOH) often couples strongly with the torsional motion of the same OH group.[6,15,47] Nevertheless, various studies have shown that excitation of a 2νOH mode can also drive the rotation of heavier molecular groups.[4,8,19,32] Two illustrative examples are 3-hydroxy-2-formyl-azirine[32] and kojic acid[19] in which excitation of the 2νOH overtones was found to induce conformational changes in the heavy hydroxymethyl and formyl fragments, respectively (Fig. 1). Investigation of the interplay between OH rotamerization and other conformational IVR redistribution pathways under matrix-isolation conditions is difficult when noble gases are used as matrix hosts, since the high-energy OH rotamers generated by IR excitation tend to relax rapidly to lower-energy forms *via* H-tunneling.[1,2,7,20,22,23,28,29,49] In contrast, when N_2 is used as host matrix, a significant enhancement of the life-time of these high-energy OH rotamers[8,20,50] occurs, through the formation of OH$\cdots$N$_2$ interactions.[51,52] This provides a more favorable environment for evaluating the efficiency of the NIR-induced OH torsional motions in comparison with other competing conformational rearrangements.

As part of a series of studies conducted in our laboratory on the NIR-induced isomerization of phenol derivatives bearing an isopropyl group attached to the phenyl ring, we investigated whether this group could undergo rotation upon excitation of the overtone of an OH stretch vibration. The model systems selected for this purpose were thymol (2-isopropyl-5-methylphenol) and carvacrol (5-isopropyl-2-methylphenol), whose structures are depicted in Fig. 2. In low-temperature noble gas matrices (Ar and Xe), the two lowest-energy conformers having the OH group pointing away from the nearest alkyl fragment (*trans*-OH, Fig. 3) and differing in the orientation of the isopropyl fragment, were spectroscopically identified.[53,54] In contrast, the higher-energy conformers, with the OH group oriented toward the nearest alkyl fragment (*cis*-OH, Fig. 3), were not detected due to their fast relaxation *via* H-tunneling rotamerization into the more stable *trans*-OH counterparts. Such behavior is consistent with previous observations for other structurally related phenol derivatives in noble gas matrices.[28,29,55]

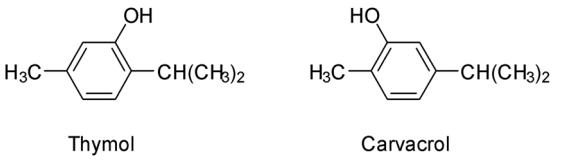

Fig. 2 Molecular structures of thymol (2-isopropyl-5-methylphenol) and carvacrol (5-isopropyl-2-methylphenol).

The conformational landscapes of thymol and carvacrol have also been investigated in the gas phase using broadband microwave spectroscopy[56,57] and laser-based jet techniques.[58] These studies enabled the identification of multiple conformers with high structural precision. These included the lowest-energy structures in which the OH group is oriented away from the nearest alkyl substituent, which were also identified in our previous studies in Ar and Xe matrices[53,54] Besides, higher-energy conformers in which the OH group points toward the alkyl fragment were also identified: one such conformer in thymol and two in carvacrol. Gas-phase approaches thus provide detailed insight into intrinsic molecular structures and relative conformer energetics under isolated, collision-free conditions, although the investigation of long-timescale conformational dynamics is challenging. In contrast, matrix-isolation infrared spectroscopy offers a complementary framework for investigating conformational interconversions over extended timescales, providing access to dynamical information that complements the structural insights obtained from gas-phase jet experiments.

Attempts to induce interconversion between the two *trans*-OH conformers (*via* rotation of the isopropyl group) using narrowband NIR light tuned to the 2ν_{OH} vibration were performed for thymol isolated in a Xe matrix. Despite the energy deposited in the molecule by the NIR radiation (7061–7047 cm^{-1}, equivalent to $\sim$84 kJ mol^{-1}) being more than three times higher than the computed isopropyl rotamerization barrier (23–26 kJ mol^{-1}, Fig. 3), no interconversion between the two conformers was observed.[54] We hypothesized that this lack of interconversion arises from preferential dissipation of vibrational energy into the OH torsional mode, whose calculated barrier is considerably lower than that for isopropyl rotation (9–14 kJ mol^{-1}, Fig. 3). To further investigate this hypothesis, the present study aims to obtain deeper insight into the mechanisms governing conformational transformations in thymol and carvacrol isolated in an N_2 matrix. Importantly, the isopropyl rotamerization barrier in carvacrol (10–11 kJ mol^{-1}) is significantly lower than in thymol and is of the same order as the OH-rotamerization barrier (11–13 kJ mol^{-1}, Fig. 3). Therefore, these molecular systems offer a valuable opportunity to evaluate whether the efficiency of NIR-induced rotamerization is dictated primarily by the barrier height or not.

In addition to the selective NIR-induced conformational interconversions, the kinetics of the spontaneous *cis*-to-*trans* OH conversion in a N_2 matrix under dark conditions were investigated for both compounds. This process is mediated by intramolecular hydrogen-atom tunneling through the rotational barrier. By tracking the temporal evolution of diagnostic vibrational bands, the depopulation rates of the *cis*-OH conformers and the associated tunneling dynamics were quantitatively characterized.

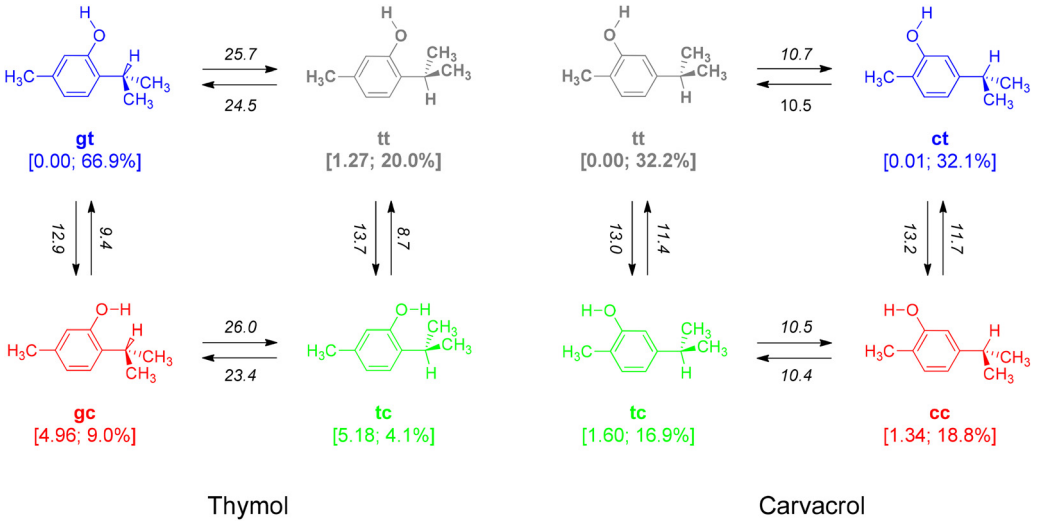

Fig. 3 Conformers of thymol (2-isopropyl-5-methylphenol) and carvacrol (5-isopropyl-2-methylphenol), along with their B3LYP/6-311++G(d,p) Gibbs free energies at 298.15 K relative to the most stable conformer and corresponding Boltzmann populations (values in squared brackets). Energy barriers (including zero-point-vibrational energy correction) for the conformational interconversions are indicated next to the arrows representing these processes. All energies are expressed in kJ mol^{-1}. Conformers are labeled using two letters [**g** (±*gauche*), **t** (*trans*), or **c** (*cis*)] where the first letter denotes the orientation of the isopropyl group and the second refers to the orientation of the hydroxyl group relative to the nearest alkyl fragment, as detailed in the text.

2. Methods

2.1. Experimental section

Solid thymol (Fluka, 99.5%), liquid carvacrol (Sigma-Aldrich, 98%), and high-purity nitrogen (Air Liquide, N50) were used in the experiments. A detailed description of the procedure and equipment used in the matrix deposition is provided elsewhere.[53,54] IR spectra of the matrix-isolated compounds were recorded with a Thermo Nicolet 6700 Fourier-transform infrared (FTIR) spectrometer both in the mid-IR (4000–400 cm^{-1}) and NIR (7500–4000 cm^{-1}) regions. In the mid-IR region, the spectra were recorded with a 0.5 cm^{-1} resolution using a deuterated triglycine sulphate (DTGS) detector and a KBr beam splitter. In the NIR region, the spectra were recorded with 1 cm^{-1} resolution using an InGaAs detector and a CaF_2 beam splitter. The NIR irradiations were undertaken *in situ* using the idle beam of a Spectra Physics Quanta-Ray optical parametric oscillator (MOPO-SL) pumped by a Nd:YAG Spectra Physics Quanta-Ray PRO-230-10 laser, providing a NIR beam with a bandwidth of 0.2 cm^{-1}, pulse frequency of 10 Hz, and an energy of ~10 mJ. The time of irradiation at a particular wavenumber was ~20 min. In some experiments, to partially protect the matrices from the high frequency broadband radiation emitted from the IR spectrometer, a longpass filter (Edmund Optics) transmitting only IR light below ~2200 cm^{-1} was used. Complete blocking of IR light (dark conditions) was achieved by placing a metal plate between the spectrometer source and the sample.

2.2. Theoretical calculations

To assist in the interpretation of the experimental IR spectra, harmonic vibrational calculations at the B3LYP[59–62]/6-311++G(d,p) level were performed for the conformers of thymol and carvacrol, using fully optimized geometries at the same level of theory. The computed harmonic wavenumbers were scaled by 0.980 and 0.945 for the regions below and above 2000 cm^{-1}, respectively. Despite the relative simplicity of this combination of functional and basis set, it has been successfully employed in our laboratory to predict the vibrational spectra of these molecules, and the calculated conformational energies compare well with those obtained at higher levels of theory, as demonstrated in our previous studies on these molecules.[53,54] Anharmonic vibrational calculations at the B3LYP/6-311++G(2d,2p) were also carried out using the fully automated second-order vibrational perturbative approach developed by Barone and co-workers.[63–65] Calculated anharmonic wavenumbers were not scaled. All calculations were performed using the Gaussian 16 program package (Rev. B.01).[66]

3. Results and discussion

3.1. Gas-phase conformational distribution and barriers for the hydroxyl and isopropyl rotamerizations

The molecular structures of carvacrol and thymol are shown in Fig. 2. They differ only by the position of the OH group relative to the alkyl fragments: in thymol it is ortho to the isopropyl group, whereas in carvacrol it is ortho to the methyl group. The conformational behavior of both molecules has been extensively studied in our laboratory using various levels of theory.[53,54] Here, we highlight only the key findings from these studies that are relevant to the present work.

Both molecules can adopt four distinct conformers, each designated by a two-letter code (Fig. 3). The first letter denotes the orientation of the tertiary C–H bond of the isopropyl

fragment relative to the C–O bond, while the second indicates the orientation of the OH group relative to the nearest alkyl fragment. The notation used is as follows: **g** (*gauche*, ~60°), **c** (*cis*, 0°), and **t** (*trans*, 180°). The relative Gibbs energies of the conformers at 298.15 K, calculated at the B3LYP/6-311++G(d,p) level, and the corresponding Boltzmann populations, are included in Fig. 3. From these data, the following conclusions can be drawn: (i) for the two molecules, the two *trans*-OH conformers (**gt** and **tt** in thymol; **tt** and **ct** in carvacrol) are more stable than their *cis*-OH counterparts (**gc** and **tc** in thymol; **tc** and **cc** in carvacrol); (ii) within each group of conformers, thymol shows a preference for the *gauche* orientation of the C–H bond over a *trans* one (the *cis* conformation is not a minimum). In carvacrol, however, the *cis* and *trans* orientations of the C–H bond are practically isoenergetic. According to the gas-phase population predictions at 298.15 K (also included in Fig. 3), thymol exists predominantly in the **gt** conformer, followed by **tt**, with a minor contribution from **gc** and a residual presence of **tc**. In contrast, carvacrol exhibits a broader conformational distribution, with the **tt** and **ct** forms being the most abundant and nearly equimolar, but the **tc** and **cc** conformers also contribute appreciably. These results are consistent with those reported by Schmitz *et al.*[67]

In addition to gas-phase population predictions, the energy barriers for conformational isomerization, included in Fig. 3, play a crucial role in determining which conformers may persist upon matrix deposition. The barriers for OH rotamerization range from 11 to 14 kJ mol^{-1} for the conversion of the *trans*-OH into the *cis*-OH conformers and from 9 to 12 kJ mol^{-1} for the reverse process. These barriers are sufficiently high to suppress conventional, temperature-dependent over-the-barrier relaxation in a cryogenic matrix. Nevertheless, because the OH-rotamerization involves the motion of a light hydrogen atom, H-tunneling can promote *cis*-OH → *trans*-OH decay. This tunneling pathway accounts for the absence of detectable *cis*-OH conformers of thymol and carvacrol in noble-gas matrices, where they are assumed to relax too rapidly to be observed spectroscopically.[53,54] By contrast, owing to the well-known stabilizing effect of N_2 as a matrix medium, the higher energy *cis*-OH conformers are more likely to be detected in N_2 matrices. Regarding the isopropyl group rotamerization, the calculated energy barriers range from 23 to 26 kJ mol^{-1} in thymol and are significantly lower in carvacrol (10–11 kJ mol^{-1}), where the increased spatial separation between the isopropyl and OH groups reduce steric hindrance. From an experimental perspective, such energy barriers, involving the movement of a bulky fragment, cannot be overcome at cryogenic temperatures (10–20 K), effectively preventing interconversion between these conformers under matrix isolation conditions.

3.2. Mid- and near-IR spectra of thymol and carvacrol isolated in solid N_2 at 15 K

The experimental mid-IR spectra (1550−745 cm^{-1}) of thymol and carvacrol, recorded immediately after their deposition in a low-temperature N_2 matrix, are shown in Fig. 4a and 5a, respectively. These spectra are slightly different from those

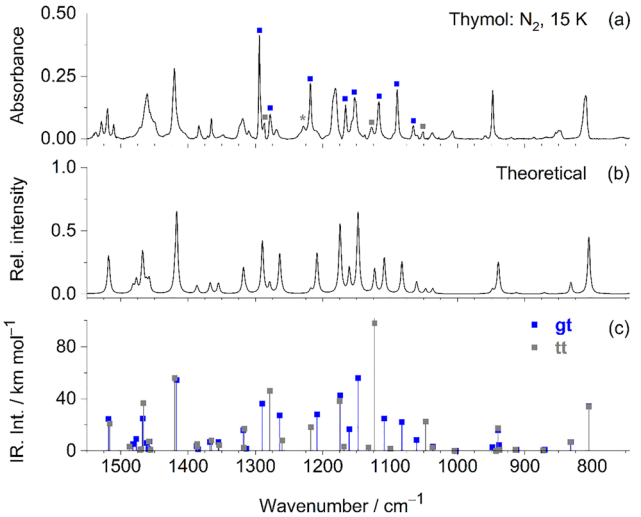

Fig. 4 (a) Experimental mid-IR spectrum of thymol recorded after isolating monomers of the compound in a N_2 matrix at 15 K. (b) Theoretical spectrum of a mixture of the **gt** and **tt** conformers, which was simulated from the B3LYP/6-311++G(d,p) vibrational calculations carried out for both conformers. Bands highlighted with blue and grey squares are assigned to the **gt** and **tt** conformers, respectively, by comparison with the computed vibrational data. The band at 1229 cm^{-1}, marked with an asterisk, is tentatively attributed to the **tt** conformer, but it may also originate from the high-energy **cc** conformer, as demonstrated by the results of the NIR irradiation experiments discussed in Section 3.3. Lorentzian functions (FWHM = 4 cm^{-1}) centered at the calculated wavenumbers were used and the intensities were scaled by 1.0 (**gt**) and 0.15 (**tt**) to best match the experimental spectrum. (c) Scaled wavenumbers and unscaled IR intensities extracted from the harmonic vibrational calculations performed for the **gt** (blue squares) and **tt** (grey squares) conformers.

recorded in noble gas matrices (see Fig. S1 and S2 in the SI for further details), with minor deviations in band positions, particularly in the OH stretching region, which is highly sensitive to matrix effects, and in the relative intensities of certain bands. To aid in the interpretation of the experimental spectra, harmonic vibrational calculations were performed at the B3LYP/6-311++G(d,p) level for the conformers predicted to be present in the matrices.

For thymol, the experimental spectrum of the freshly deposited N_2 matrix at 15 K (Fig. 4a) is very well reproduced by the theoretical spectrum simulated from a mixture of the **gt** and **tt** conformers (Fig. 4b). This spectrum was simulated from the vibrational data computed for both conformers, with the relative intensities of **gt** and **tt** scaled by 1.0 and 0.15, respectively, to achieve a good agreement with the experimental data. Although the calculated stick IR spectra of the two conformers are overall quite similar (Fig. 4c), some bands in the 1300–1000 cm^{-1} region can be unambiguously assigned to the dominant **gt** conformer (see Fig. S3 for details). These include the features at 1295, 1278, 1218, 1166, 1154, 1117, 1090, and 1065 cm^{-1}. In contrast, the experimental identification of the **tt** conformer is considerably more challenging, since most of its IR features overlap with those of the most abundant **gt** conformer. Nevertheless, subtle shoulders at 1286, 1229 and 1127 cm^{-1}, as well as the weak band at 1051 cm^{-1}, can

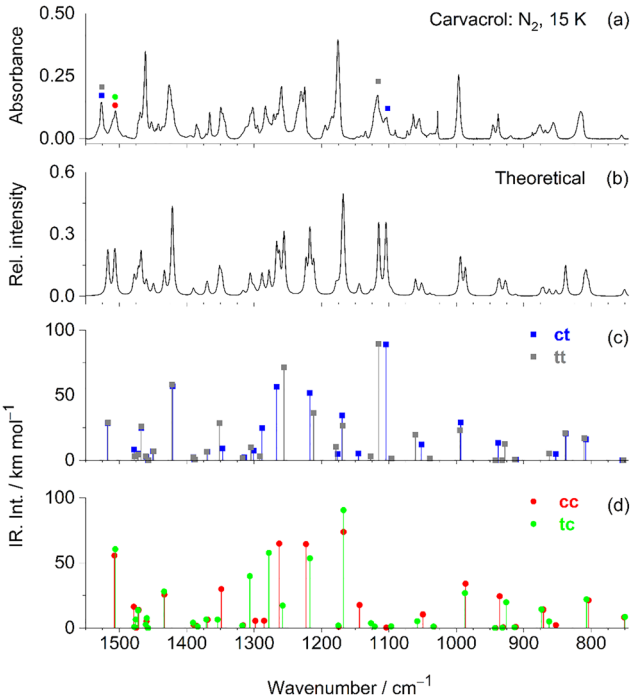

Fig. 5 (a) Experimental mid-IR spectrum of carvacrol recorded after isolating monomers of the compound in a N_2 matrix at 15 K. (b) Theoretical spectrum of a mixture of the **tt**, **ct**, **tc** and **cc** conformers, which was simulated from the B3LYP/6-311++G(d,p) vibrational calculations carried out for each species. Lorentzian functions (FWHM = 4 cm^{-1}) centered at the calculated wavenumbers were used and the intensities were scaled by 1 : 1 : 0.5 : 0.6 to best match the experimental spectrum. (c and d) Scaled wavenumbers and unscaled IR intensities extracted from the harmonic vibrational calculations performed for the **ct** (blue squares), **tt** (grey squares), **cc** (red circles) conformers. **tc** (green circles).

be tentatively attributed to the **tt** form (Fig. S3). Notably, its strongest absorption predicted at 1123 cm^{-1} (A^{th} = 111.8 km mol^{-1}) has a very weak experimental counterpart at 1127 cm^{-1}. This provides further evidence for the significantly lower abundance of the **tt** form in the deposited N_2 matrix as compared with the **gt** conformer, in line with the theoretical predictions.

Regarding carvacrol, the spectroscopic identification of individual conformers in the deposited N_2 matrix (Fig. 5a), by comparison with the calculated spectra (Fig. 5b and c), proves even more challenging than in the case of thymol. This difficulty arises because all four conformers have appreciable gas-phase populations and display very similar spectral profiles. The only reliable markers are the doublets observed at 1527/1507 cm^{-1} and 1117/1104 cm^{-1}. In the first case, the higher-frequency component can be attributed to the two most stable conformers **tt** and **ct**, whereas the lower-frequency one corresponds to the higher-energy forms **tc** and **cc**. The second doublet occurs in a spectral region where only the two lower-energy conformers absorb, and their predicted bands do not overlap. Thus, the higher- and lower-frequency components of this doublet can be assigned to the **tt** and **ct** conformers, respectively.

In summary, the spectral analysis of matrix isolated thymol and carvacrol confirms the presence of the most stable *trans*-OH conformers in the matrix and, due to the stabilizing effect of the N_2 matrix as compared to the noble gas matrices, suggests the possible presence of the high-energy *cis*-OH conformers in carvacrol. However, the strong spectral overlap prevents an unambiguous identification of the conformers. This limitation underscores the importance of complementary techniques, such as selective NIR vibrational excitation, to manipulate and probe conformational populations. The results of these NIR irradiation experiments are presented in Section 3.3 and based on these results comprehensive spectral assignments are provided in Tables S1–S4.

The IR spectra of thymol and carvacrol isolated in solid N_2 were also recorded in the near-IR region (7500–4000 cm^{-1}) to determine the positions of the OH-stretching overtone (2νOH) bands, which are required for selecting the wavenumbers for NIR irradiations. In both compounds, the 2νOH absorption appears as a broad band from 7110 to 7060 cm^{-1}, centered at ~7082 cm^{-1} (Fig. 6c and d), which mirrors the νOH band profile centered at ~3625 cm^{-1} (Fig. 6e and f). Anharmonic frequency calculations at the B3LYP/6-311++G(2d,2p) are in good agreement with the experimental data. For thymol, 2νOH transitions are predicted at 7128 and 7145 cm^{-1} for the **gt** and **tt** conformers, respectively, while for carvacrol, the four conformers overlap more strongly, with 2νOH transitions between 7129 and 7132 cm^{-1}.

3.3. Conformational conversions induced by NIR laser-light irradiations

Due to the relatively broad profile of the $2\nu_{OH}$ overtone bands, in the irradiation experiments, narrowband NIR light was tuned not only at the wavenumber corresponding to the band center but also at wavenumbers slightly offset to the higher- and lower-frequency sides. This approach ensured that the laser beam, with its narrower bandwidth compared to the overtone band, effectively targeted multiple spectral positions within the $2\nu_{OH}$ absorption profile to maximize selectivity. The changes triggered by the NIR irradiations were monitored by collecting mid-IR spectra.

3.3.1. Thymol. The first set of irradiation experiments was performed by tuning the laser to 7102 cm^{-1}, followed by 7082 cm^{-1}, corresponding respectively to the high-frequency side and the center of the 2νOH band. Exposing matrix-isolated thymol to NIR radiation at these wavenumbers for approximately 20 minutes each resulted in similar spectral changes (more pronounced upon irradiation at the lower wavenumber), indicating the occurrence of conformational isomerization. These spectral changes are reflected in the difference IR spectrum shown in Fig. 7b, obtained by subtracting the pre-irradiation spectrum from the post-irradiations' spectrum. As illustrated in this difference spectrum, these irradiations resulted in an increase in the intensity of a specific set of bands (highlighted with red circles) alongside a simultaneous decrease in the intensity of another set of bands (marked with blue squares). These observations provide clear evidence of

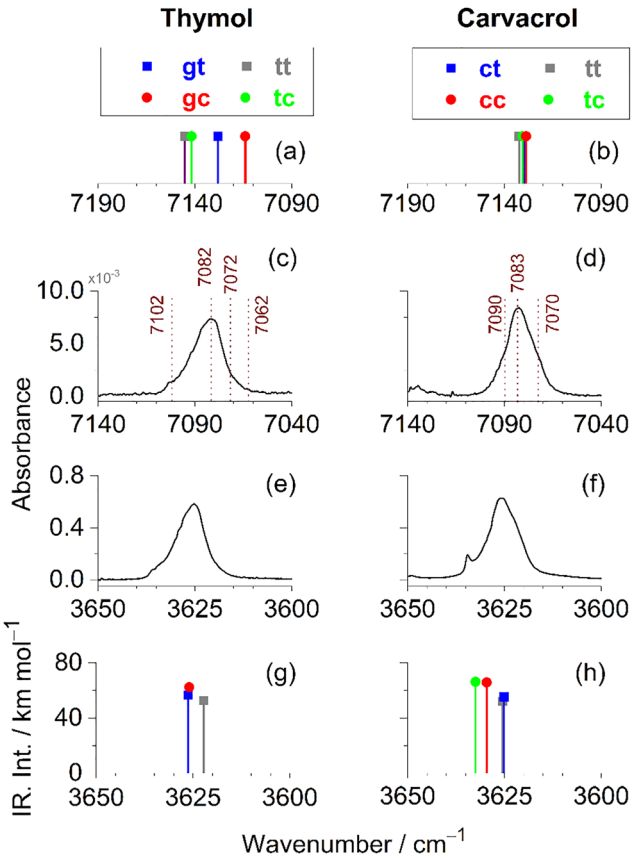

Fig. 6 Fragments of the near-IR (c and d) and mid-IR (e and f) spectra of thymol and carvacrol isolated in solid N_2 at 15 K showing the $2\nu_{OH}$ and ν_{OH} absorption bands, respectively. The dotted vertical lines in panels (c) and (d) indicate the wavenumbers applied in the narrowband NIR irradiations of the matrix isolated compounds. The $2\nu_{OH}$ and ν_{OH} absorption bands are compared with results of anharmonic (a and b) and harmonic (g and h) vibrational calculations carried out at the B3LYP/6-311++G(2d,2p) and B3LYP/6-311++G(d,p) levels of theory, respectively, for the conformers of both molecules. The ν_{OH} mode computed for the **tc** conformer of thymol (3652.3 cm^{-1}; *A*th = 83.9 km mol^{-1}) is not shown as it is predicted outside of the spectral range shown. Anharmonic wavenumbers are unscaled while the harmonic ones were scaled by 0.945.

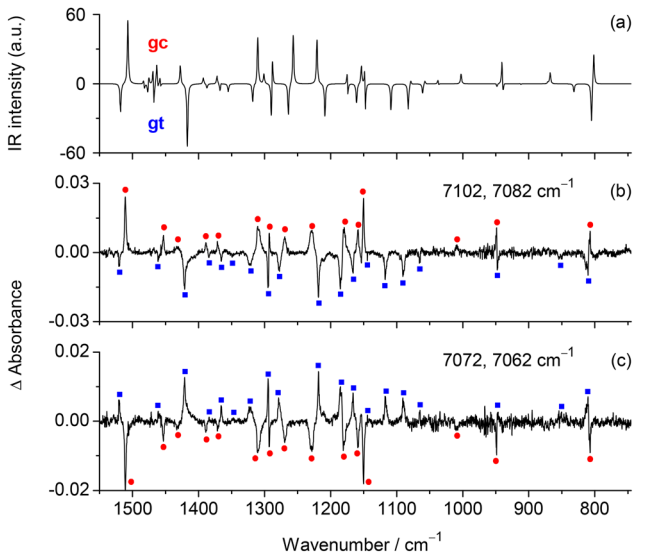

Fig. 7 Spectral indication of conformational changes in thymol isolated in solid N_2 (15 K) following excitation of the 2νOH mode, supported by simulated IR spectra of the involved conformers. (b) Spectrum recorded after a total of 40 min of NIR irradiations at 7102 and 7082 cm^{-1} (20 minutes each) minus that recorded before the irradiations (positive bands indicate conformer formation upon irradiation). (c) Spectrum recorded after a total of 40 min of NIR irradiations at 7072 and 7062 cm^{-1} (20 minutes each) minus that recorded before these irradiations (positive bands indicate conformer formation upon the irradiations). (a) B3LYP/6-311++G(d,p) simulated IR difference spectrum for the conversion of conformer **gt** to **gc** (intensity ratio 1 : 1).

NIR-induced conformational changes taking place in matrix-isolated thymol.

Subsequent irradiations were conducted on the lower-frequency side of the 2νOH profile, specifically at 7072 and 7062 cm^{-1}. The results of these irradiations, as reflected in the difference spectrum shown in Fig. 7c, reveal that the bands which had previously increased in intensity now displayed a clear decrease, while those that had decreased in intensity showed a corresponding increase. This reversal in the spectral behavior unequivocally demonstrates that excitation at 7072 and 7062 cm^{-1} induces the opposite conformational transformation(s) to those triggered by excitation at the 7102 and 7082 cm^{-1}.

To support the assignment of the conformers being consumed or produced during the NIR irradiations, the experimental difference spectra were compared with the B3LYP/6-311++G(d,p) theoretical spectra of all four thymol conformers. This analysis revealed that the spectral changes induced by NIR irradiation are well reproduced by the theoretical difference spectrum **gc** minus **gt**, shown in Fig. 7a. Accordingly, irradiations at 7102 and 7082 cm^{-1} promote the **gt** → **gc** conversion, while irradiations at 7072 and 7062 cm^{-1} induce the reverse **gc** → **gt** transition, in agreement with the anharmonic vibrational calculations which predict the 2νOH overtone of **gt** conformer at a higher frequency than that of **gc**. This bidirectional behavior provides evidence of the reversible nature of the NIR-induced conformational interconversion, as illustrated in Fig. 8. The spectral signatures of the **gt** and **gc** conformers, extracted from the experimental difference spectra shown in Fig. 7, are listed in Tables S1 and S2, respectively. These tables also include approximate assignments of the corresponding vibration modes.

It is important to note that no spectral evidence of interconversion between the **gt** and **tt** conformers was detected upon excitation of the $2\nu_{OH}$ mode, consistent with our previous results

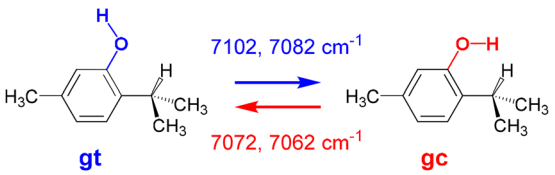

Fig. 8 Bidirectional NIR-induced OH-rotamerization observed for thymol isolated in a low temperature N_2 matrix.

in a Xe matrix.[54] This confirms that isopropyl rotamerization does not occur under these conditions, suggesting that energy redistribution within the molecule preferentially channels into the OH-rotamerization rather than facilitating the isopropyl group rotation.

Furthermore, no spectral indication of interconversion between the **tt** and **tc** conformers were observed. This conclusion is supported by a detailed analysis of the spectral changes in the 1300–1000 cm^{-1} region where, as mentioned above, conformer **tt** shows weak absorptions at 1286, 1129 and 1051 cm^{-1}. Notably, these three bands remain unaffected by NIR irradiations at 7102 and 7082 cm^{-1} (see Fig. S4 for details). One possible explanation is that the **tt** conformer is not effectively excited during the laser irradiation; however, this is unlikely given that the entire 2νOH band profile was scanned. A more plausible hypothesis is that **tt** is indeed converted to **tc** upon NIR excitation, but the latter rapidly relaxes back to **tt** *via* H-atom tunneling, which prevents any observable net change in the **tt** population under steady-state conditions. This interpretation is consistent with the tunneling decay results, which will be presented and discussed in Section 3.4.

3.3.2. Carvacrol. Irradiation experiments were also carried out on carvacrol isolated in an N_2 matrix. The sample was exposed to the OPO tunable narrowband light at 7090, 7083, and 7072 cm^{-1}, corresponding to the high-frequency edge, maximum, and low-frequency edge of the 2νOH absorption band, respectively, for about 20 minutes each. Mid-IR spectra were recorded after each irradiation, and the resulting spectral changes are presented in Fig. 9.

Comparison of the theoretical and experimental difference spectra clearly shows the occurrence of the **tt** → **tc** and **ct** → **cc** isomerizations upon irradiation at 7090 or 7083 cm^{-1}, whereas the reverse transformations are promoted by irradiation at 7072 cm^{-1} (Fig. 10). These spectral changes provide clear evidence for the presence of two sets of conformers in the N_2 matrix, namely **tt** + **ct** and **tc** + **cc**. When this result is considered together with the spectral indication of the presence of the **tt** and **ct** conformers in the as-deposited matrix (supported by the doublet at 1117/1104 cm^{-1}), and with the fact that several of the bands that increase upon the irradiations at 7090/7083 cm^{-1} were already discernible in the pre-irradiation spectrum, taken together, the data strongly support the presence of all four conformers in the N_2 matrix, consistently with the theoretical predictions. Nevertheless, the conformer-by-conformer assignment remains less definitive than in the case of thymol. The assignment of the experimental spectra to the two conformer sets is provided in Tables S3 and S4.

It is important to note that, as in the case of thymol, we were unable to identify spectral features associated with isopropyl group rotamerization, which would lead to interconversion between the **tt** and **ct** conformers or between the **tc** and **cc** conformers. This result is particularly striking, as one might initially expect that excitation of the 2νOH overtone in carvacrol would induce isopropyl isomerization, given that its barrier is much lower than in thymol (by a factor of ~2.5) and is of the same order as that for the OH rotamerization (with the caveat that rotation of the bulky isopropyl group may be partially hindered in an N_2 matrix). The most plausible explanation is that the initially excited state, namely the OH-stretching overtone, couples more efficiently, *via* anharmonic IVR, to motions involving the hydroxyl group, in particular to the OH torsional coordinate. The behaviour of carvacrol is therefore consistent with a mode-selective process, whereby excitation of the 2νOH overtone preferentially drives OH-rotamerization.

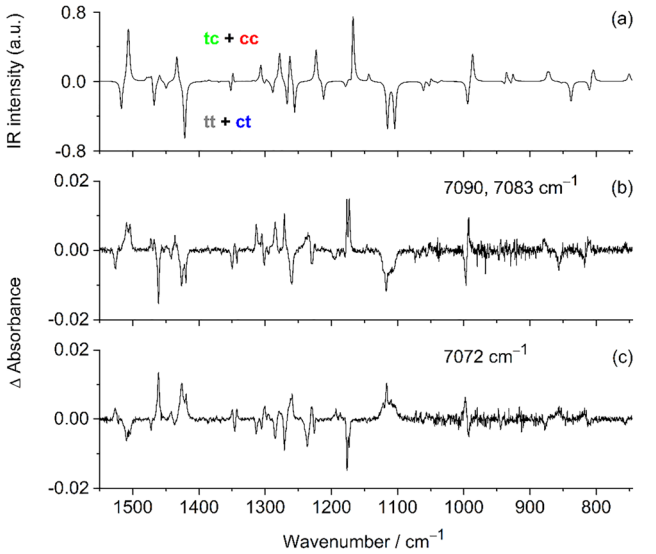

Fig. 9 Spectral indication of conformational changes in carvacrol isolated in solid N_2 (15 K) following excitation of the $2\nu_{OH}$ mode, supported by simulated IR spectra of the involved conformers. (b) Spectrum recorded after a total of 20 min of NIR irradiations at 7090 or 7083 cm^{-1} minus that recorded before these irradiations (positive bands indicate conformer formation upon irradiation). (c) Spectrum recorded after a total of 20 min of NIR irradiations at 7072 cm^{-1} minus that recorded before these irradiations (positive bands indicate conformer formation upon the irradiations). (a) B3LYP/6-311++G(d,p) simulated IR difference spectrum for the conversion of conformers **tt** + **ct** into conformers **tc** + **cc** (intensity ratio 1 : 1).

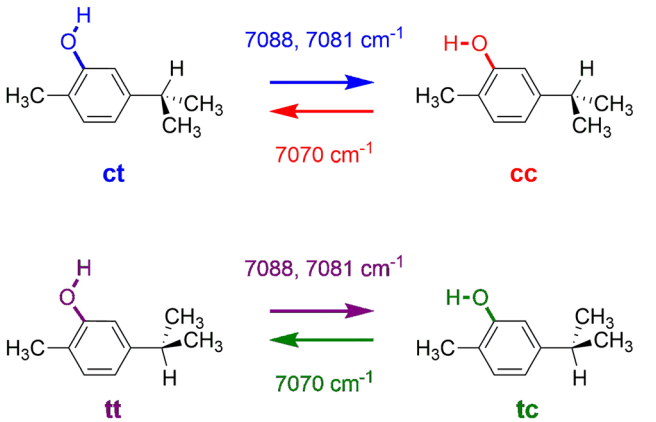

Fig. 10 Bidirectional NIR-induced OH-rotamerization observed for carvacrol isolated in a low-temperature N_2 matrix.

3.4. Decay of the higher-energy *cis*-OH conformers under dark conditions

Once the high-energy conformers were generated by selective excitation of the 2νOH overtones of their low-energy counterparts (7102 and 7082 cm^{-1} for thymol, and 7090 and 7083 cm^{-1} for carvacrol), the sample was maintained under dark conditions for approximately one hour. During this period, a limited number of IR spectra were collected using a 2200 cm^{-1} cutoff filter and restricting each acquisition to 32 scans, thereby minimizing exposure to residual spectrometer radiation and preventing any unwanted photoinduced processes. The spectral changes observed under these conditions, shown in Fig. 11, provide unambiguous evidence that the higher-energy *cis*-OH conformers (**gc** in thymol; **tc** and **cc** in carvacrol) decay into their lower-energy *trans*-OH counterparts (**gt** in thymol; **tt** and **ct** in carvacrol) by means of H-atom tunneling.

To quantitatively monitor the kinetics of the OH-rotamerization tunneling, specific diagnostic bands were selected: the band at 1310 cm^{-1} for thymol, which is assigned to the **gc** conformer (see Table S2), and the band at 1507 cm^{-1} for carvacrol, attributed to the **tc** and **cc** conformers (see Table S4). The time-dependent changes of the integrated absorbances (A) of the selected bands were fitted to a first-order kinetic model, $[A](t)/[A]_0 = e^{-kt}$, where $[A](t)$ and $[A]_0$ represent the absorbance of the diagnostic band at time t and initially, respectively, and from these fits the tunneling rate constants were estimated (Fig. 12). For thymol, a tunneling rate constant of $(8.4 \pm 0.4) \times 10^{-4}$ s^{-1} was determined, corresponding to a half-life of ~14 minutes. In the case of carvacrol, a tunneling rate constant of $(5.4 \pm 0.3) \times 10^{-4}$ s^{-1} was obtained, corresponding to a half-life of ~21 minutes. The rapid conversion of the high-energy *cis*-OH rotamers into the more stable *trans*-OH forms indicates that the *cis*-OH → *trans*-OH isomerization previously observed under NIR irradiation is also driven by an H-tunneling mechanism.

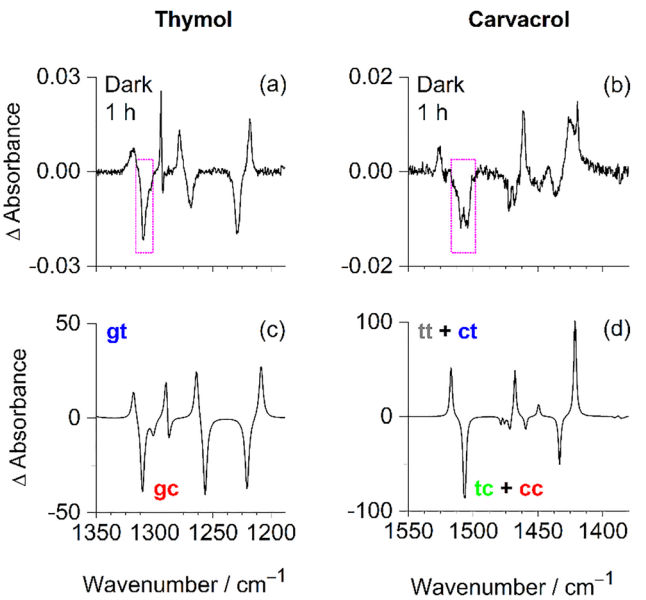

Fig. 11 (a and b) Fragments of experimental difference spectra showing the spectral changes observed after keeping matrix-isolated thymol and carvacrol (N_2, 15 K) in dark for 1 hour. Prior to the dark period, the samples were enriched in the higher-energy *cis*-OH conformers by NIR laser irradiations at 7082 cm^{-1} (thymol) or 7082 cm^{-1} (carvacrol). The negative bands enclosed by a dotted rectangle were used to monitor the kinetics of the dark process. (c and d) B3LYP/6-311++G(d,p) theoretical difference spectra illustrating the conversion of the higher-energy *cis*-OH conformers into the lower-energy *trans*-OH conformers.

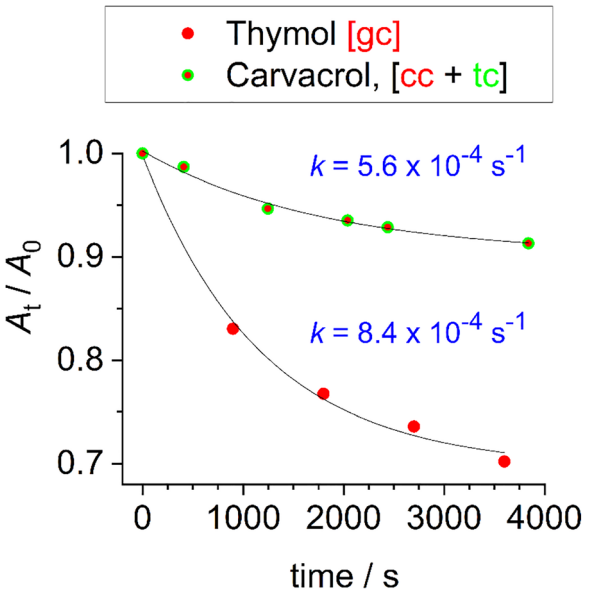

Fig. 12 Time evolution of the high-energy **gc** conformer of thymol (red circles in the lower curve) and of the high-energy **cc** and **tc** conformers of carvacrol (green circles with red-filled centers in the upper curve) under dark conditions. The decay was monitored by integrating the vibrational bands at 1310 cm^{-1} (thymol) and 1507 cm^{-1} (carvacrol). Absorbances measured after 15 h in the dark, when no further spectral changes occurred, were subtracted from the time-dependent values to correct for the non-reactive conformers (70% for thymol and 90% for carvacrol). The corrected absorbances (A_t) were normalized to the initial absorbances (A_0) to obtain the relative populations of the reactive conformers. Solid lines represent the best single-exponential fits to the experimental data for carvacrol and thymol, respectively (R^2 = 0.99).

The estimated values are comparable to OH-rotamerization tunneling rates reported for other phenol derivatives under similar experimental conditions, such as 2-cyanophenol[28] and 2-isocyanophenol.[29] The slightly slower OH-rotamerization tunneling rate observed for carvacrol in relation to thymol is consistent with the qualitative trend in the calculated *cis*-OH → *trans*-OH barriers shown in Fig. 3 (11–12 kJ mol^{-1} for **cc** → **ct** and **tc** → **tt** in carvacrol compared to 9 kJ mol^{-1} for **gc** → **gt** in thymol, Fig. 3).

In our previous study on thymol, we have computed the tunneling probabilities for the **gc** → **gt** and **tc** → **tt** conversions in gas phase, and from these values, the corresponding tunneling rates and half-lives were derived. It was found that the half-life time of the **gc** → **gt** process is approximately 12.5 times longer than that of the **tc** → **tt** process, reflecting a more efficient tunneling pathway in the latter case. Assuming that

a similar ratio holds under N_2 matrix isolation conditions, the expected half-life for the **tc** → **tt** conversion would be on the order of ~1 minute. This rapid decay provides a consistent explanation for the experimental observation reported above that the bands attributed to the **tt** conformer remain essentially unaffected by the NIR irradiations. In fact, if the **tc** conformer is photogenerated under these conditions, it would promptly relax back to **tt** on a timescale too short to be spectroscopically detected.

4. Concluding discussion

Carvacrol and thymol were isolated in an N_2 cryogenic matrix at 15 K. Spectroscopic analysis provided evidence for the presence of the lower-energy *trans*-OH conformers (**gt** and **tt** in thymol; **tt** and **ct** in carvacrol) in the as-deposited matrix for both molecules. Higher-energy *cis*-OH conformers were observed only for carvacrol (**tc** and **cc**).

Excitation of the 2νOH overtones of the *trans*-OH conformers with NIR laser light induced the **gt** → **gc** process in thymol and the **tt** → **tc** and **ct** → **cc** processes in carvacrol. These findings demonstrate that the energy absorbed in the first OH-stretch overtone is efficiently channeled into the torsional coordinate, driving rotamerization of the same hydroxyl group. Furthermore, these OH-induced interconversions could be selectively reversed by fine-tuning the irradiation frequency. No evidence of isopropyl group rotamerization was detected in either compound. While this outcome was somehow expected for thymol given that the energy barrier for isopropyl rotation is significantly higher than that for OH-rotamerization, it is unexpected in the case of carvacrol, where the isopropyl rotational barrier is lower than in thymol and comparable to the OH-rotamerization barrier. These results demonstrate that regardless of the magnitude of the energy barriers for the internal rotation of the hydroxyl and isopropyl groups, IVR preferentially couples the excited 2νOH mode to the local OH-rotamerization coordinate rather than the C_3H_7-rotamerization coordinate.

Finally, the kinetic measurements performed in dark provided unambiguous evidence that the high-energy *cis*-OH revert to their more stable *trans*-OH forms through OH-rotamerization tunneling. The estimated tunneling rate constants were approximately 8×10^{-4} s^{-1} for thymol and 5×10^{-4} s^{-1} for carvacrol, respectively, corresponding to half-life times of about 14 and 21 minutes, respectively. These values consistent with those reported for related phenolic systems. From the experimental results obtained for thymol and previous tunneling calculations performed for this molecule in vacuum, which predicted that the **tc** → **tt** process proceeds roughly 12.5 times faster than the **gc** → **gt** one, the half-life of the **tc** → **tt** conversion in the N_2 matrix can be estimated to be approximately one minute. This likely accounts for the apparent stability of the **tt** conformer during NIR irradiation, as any transient **tc** population would decay too rapidly to be detected experimentally.

Conflicts of interest

There are no conflicts to declare.

Data availability

The authors confirm that the data supporting the findings of this study are available within the article and its supplementary information (SI). All data necessary for reproducing the calculations, including optimized structures, are presented in the SI, where the reader can also find figures and tables with experimental data supporting our findings. Supplementary information available. See DOI: https://doi.org/10.1039/d5cp04677g.

All data gathered during the experiments are available from the corresponding author, AJLJ, or the author LJD, upon request.

Acknowledgements

L. J. D. (postdoctoral fellowship #2022/09269-1) and A. A. C. B. (grant #2015/01491-3) are grateful to the São Paulo Research Foundation (FAPESP) for financial support. A. A. C. B. also thanks the Conselho Nacional de Desenvolvimento Científico e Tecnológico (CNPq) of Brazil for academic support (Grant #313720/2023-1). R. F. thanks the Horizon-Widera-2023-Talents-01 ERA-Chair 1011848998 Spectroscopy@IKU "*Manipulating and Characterizing Molecular Architectures: From Isolated Molecules to Molecular Crystals*" (Funded by the European Union) for financial support. The authors acknowledge the Coimbra Chemistry Centre – Institute of Molecular Sciences (CQC-IMS) which is supported by the Fundação para a Ciência e a Tecnologia (FCT), Portuguese Agency for Scientific Research. CQC is funded by FCT through projects UID/PRR/00313/2025 (https://doi.org/10.54499/UID/PRR/00313/2025) and UID/00313/2025 (https://doi.org/10.54499/UID/00313/2025) and IMS through special complementary funds provided by FCT (project LA/P/0056/2020 https://doi.org/10.54499/LA/P/0056/2020). The authors also acknowledge the Laboratory for Advanced Computing at University of Coimbra (UC-LCA) for providing computing resources that have contributed to the research results reported within this paper, and Coimbra Laser Lab (CLL) for providing experimental facilities.

References

1 M. Pettersson, J. Lundell, L. Khriachtchev and M. Räsänen, IR spectrum of the other rotamer of formic acid, *cis*-HCOOH, *J. Am. Chem. Soc.*, 1997, **119**(48), 11715–11716, DOI: 10.1021/ja972362l.

2 M. Pettersson, E. M. S. Maçôas, L. Khriachtchev, J. Lundell, R. Fausto and M. Räsänen, *cis* → *trans* conversion of formic acid by dissipative tunneling in solid rare gases: influence of environment on the tunneling rate, *J. Chem. Phys.*, 2002, **117**(20), 9095–9098, DOI: 10.1063/1.1521429.

3 E. M. S. Maçôas, L. Khriachtchev, M. Pettersson, R. Fausto and M. Räsänen, Rotational isomerism in acetic acid: the

first experimental observation of the high-energy conformer, *J. Am. Chem. Soc.*, 2003, **125**(52), 16188–16189, DOI: 10.1021/ja038341a.

4 E. M. S. Maçôas, L. Khriachtchev, M. Pettersson, R. Fausto and M. Räsänen, Internal rotation in propionic acid: near-infrared-induced isomerization in solid argon, *J. Phys. Chem. A*, 2005, **109**(16), 3617–3625, DOI: 10.1021/jp044070u.

5 E. M. S. Maçôas, L. Khriachtchev, M. Pettersson, R. Fausto and M. Räsänen, Rotational isomerization of small carboxylic acids isolated in argon matrices: tunnelling and quantum yields for the photoinduced processes, *Phys. Chem. Chem. Phys.*, 2005, **7**(5), 743–749, DOI: 10.1039/B416641H.

6 I. Reva, C. M. Nunes, M. Biczysko and R. Fausto, Conformational switching in pyruvic acid isolated in Ar and N_2 matrixes: spectroscopic analysis, anharmonic simulation, and tunneling, *J. Phys. Chem. A*, 2015, **119**(11), 2614–2627, DOI: 10.1021/jp509578c.

7 N. Kuş and R. Fausto, Effects of the matrix and intramolecular interactions on the stability of the higher-energy conformers of 2-fluorobenzoic acid, *J. Chem. Phys.*, 2017, **146**(12), 124305, DOI: 10.1063/1.4978794.

8 A. Halasa, L. Lapinski, I. Reva, H. Rostkowska, R. Fausto and M. J. Nowak, Near-infrared laser-induced generation of three rare conformers of glycolic acid, *J. Phys. Chem. A*, 2014, **118**(30), 5626–5635, DOI: 10.1021/jp5051589.

9 A. Halasa, L. Lapinski, H. Rostkowska, I. Reva and M. J. Nowak, Tunable diode lasers as a tool for conformational control: the case of matrix-isolated oxamic acid, *J. Phys. Chem. A*, 2015, **119**(11), 2203–2210, DOI: 10.1021/jp501448m.

10 R. F. G. Apóstolo, G. Bazsó, R. R. F. Bento, G. Tarczay and R. Fausto, The first experimental observation of the higher-energy trans conformer of trifluoroacetic acid, *J. Mol. Struct.*, 2016, **1125**, 288–295, DOI: 10.1016/j.molstruc.2016.06.077.

11 R. F. G. Apóstolo, G. Bazsó, G. Ogruc-Ildiz, G. Tarczay and R. Fausto, Near-infrared *in situ* generation of the higher-energy *trans* conformer of tribromoacetic acid: observation of a large-scale matrix-site changing mediated by conformational conversion, *J. Chem. Phys.*, 2018, **148**(4), 044303, DOI: 10.1063/1.5010288.

12 G. Bazsó, S. Góbi and G. Tarczay, Near-infrared radiation induced conformational change and hydrogen atom tunneling of 2-chloropropionic acid in low-temperature Ar matrix, *J. Phys. Chem. A*, 2012, **116**(20), 4823–4832, DOI: 10.1021/jp212597y.

13 C. Araujo-Andrade, I. Reva and R. Fausto, Tetrazole acetic acid: tautomers, conformers, and isomerization, *J. Chem. Phys.*, 2014, **140**(6), 064306, DOI: 10.1063/1.4864119.

14 J. P. Wagner, H. P. Reisenauer, V. Hirvonen, C.-H. Wu, J. L. Tyberg, W. D. Allen and P. R. Schreiner, Tunnelling in carbonic acid, *Chem. Commun.*, 2016, **52**(50), 7858–7861, DOI: 10.1039/C6CC01756H.

15 E. M. S. Maçôas, R. Fausto, M. Pettersson, L. Khriachtchev and M. Räsänen, Infrared-induced rotamerization of oxalic acid monomer in argon matrix, *J. Phys. Chem. A*, 2000, **104**(30), 6956–6961, DOI: 10.1021/jp000634s.

16 E. M. S. Maçôas, R. Fausto, J. Lundell, M. Pettersson, L. Khriachtchev and M. Räsänen, Conformational analysis and near-infrared-induced rotamerization of malonic acid in an argon matrix, *J. Phys. Chem. A*, 2000, **104**(50), 11725–11732, DOI: 10.1021/jp002853j.

17 E. M. S. Maçôas, R. Fausto, J. Lundell, M. Pettersson, L. Khriachtchev and M. Räsänen, A matrix isolation spectroscopic and quantum chemical study of fumaric and maleic acid, *J. Phys. Chem. A*, 2001, **105**(15), 3922–3933, DOI: 10.1021/jp003802p.

18 B. Kovács, N. Kuş, G. Tarczay and R. Fausto, Experimental evidence of long-range intramolecular vibrational energy redistribution through eight covalent bonds: NIR irradiation induced conformational transformation of *E*-glutaconic acid, *J. Phys. Chem. A*, 2017, **121**(18), 3392–3400, DOI: 10.1021/acs.jpca.7b00615.

19 A. Halasa, I. Reva, L. Lapinski, H. Rostkowska, R. Fausto and M. J. Nowak, Conformers of kojic acid and their near-IR-induced conversions: long-range intramolecular vibrational energy transfer, *J. Phys. Chem. A*, 2016, **120**(17), 2647–2656, DOI: 10.1021/acs.jpca.6b01275.

20 L. Lapinski, I. Reva, H. Rostkowska, A. Halasa, R. Fausto and M. J. Nowak, Conformational transformation in squaric acid induced by near-IR laser light, *J. Phys. Chem. A*, 2013, **117**(25), 5251–5259, DOI: 10.1021/jp402128g.

21 G. Bazsó, G. Magyarfalvi and G. Tarczay, Near-infrared laser induced conformational change and UV laser photolysis of glycine in low-temperature matrices: observation of a short-lived conformer, *J. Mol. Struct.*, 2012, **1025**, 33–42, DOI: 10.1016/j.molstruc.2012.04.066.

22 G. Bazsó, G. Magyarfalvi and G. Tarczay, Tunneling lifetime of the *Ttc*/VIp conformer of glycine in low-temperature matrices, *J. Phys. Chem. A*, 2012, **116**(43), 10539–10547, DOI: 10.1021/jp3076436.

23 C. M. Nunes, L. Lapinski, R. Fausto and I. Reva, Near-IR laser generation of a high-energy conformer of L-alanine and the mechanism of its decay in a low-temperature nitrogen matrix, *J. Chem. Phys.*, 2013, **138**(12), 125101, DOI: 10.1063/1.4795823.

24 E. E. Najbauer, G. Bazsó, R. Apóstolo, R. Fausto, M. Biczysko, V. Barone and G. Tarczay, Identification of serine conformers by matrix-isolation IR spectroscopy aided by near-infrared laser-induced conformational change, 2D correlation analysis, and quantum mechanical anharmonic computations, *J. Phys. Chem. B*, 2015, **119**(33), 10496–10510, DOI: 10.1021/acs.jpcb.5b05768.

25 L. Lapinski, M. J. Nowak, I. Reva, H. Rostkowska and R. Fausto, NIR-laser-induced selective rotamerization of hydroxy conformers of cytosine, *Phys. Chem. Chem. Phys.*, 2010, **12**(33), 9615, DOI: 10.1039/c0cp00177e.

26 A. Halasa, L. Lapinski, H. Rostkowska and M. J. Nowak, Intramolecular vibrational energy redistribution in 2-thiocytosine: SH rotamerization induced by near-IR selective excitation of NH_2 stretching overtone, *J. Phys. Chem. A*, 2015, **119**(35), 9262–9271, DOI: 10.1021/acs.jpca.5b06221.

27 L. Lapinski, I. Reva, H. Rostkowska, R. Fausto and M. J. Nowak, Near-IR-induced, UV-induced, and spontaneous isomerizations in 5-methylcytosine and 5-fluorocytosine, *J. Phys. Chem. B*, 2014, **118**(11), 2831–2841, DOI: 10.1021/jp411423c.

28 A. J. Lopes Jesus, C. M. Nunes, I. Reva, S. M. V. Pinto and R. Fausto, Effects of entangled IR radiation and tunneling on the conformational interconversion of 2-cyanophenol, *J. Phys. Chem. A*, 2019, **123**(20), 4396–4405, DOI: 10.1021/acs.jpca.9b01382.

29 A. J. Lopes Jesus, I. Reva, C. M. Nunes, J. P. L. Roque, S. M. V. Pinto and R. Fausto, Kinetically unstable 2-isocyanophenol isolated in cryogenic matrices: vibrational excitation, conformational changes and spontaneous tunneling, *Chem. Phys. Lett.*, 2020, **747**, 137069, DOI: 10.1016/j.cplett.2019.137069.

30 A. J. Lopes Jesus, I. Reva, C. Araujo-Andrade and R. Fausto, Conformational switching by vibrational excitation of a remote NH bond, *J. Am. Chem. Soc.*, 2015, **137**(45), 14240–14243, DOI: 10.1021/jacs.5b08588.

31 A. J. Lopes Jesus, R. Fausto and I. Reva, Conformational changes in 5-methoxyindole: effects of thermal, vibrational, and electronic excitations, *J. Phys. Chem. A*, 2017, **121**(18), 3372–3382, DOI: 10.1021/acs.jpca.7b01713.

32 A. J. Lopes Jesus, M. C. Nunes, R. Fausto and I. Reva, Conformational control over an aldehyde fragment by selective vibrational excitation of interchangeable remote antennas, *Chem. Commun.*, 2018, **54**(38), 4778–4781, DOI: 10.1039/C8CC01052H.

33 A. Sharma, I. Reva and R. Fausto, Conformational switching induced by near-infrared laser irradiation, *J. Am. Chem. Soc.*, 2009, **131**(25), 8752–8753, DOI: 10.1021/ja903211f.

34 L. Lapinski, I. Reva, H. Rostkowska, A. J. Lopes Jesus, S. M. Vieira Pinto, R. Fausto and M. J. Nowak, Conformational isomerizations by rotation around C–C or C–N bonds: a comparative study on matrix-isolated glycolamide and *N*-hydroxyurea excited with near-IR laser light, *J. Phys. Chem. A*, 2019, **123**(17), 3831–3839, DOI: 10.1021/acs.jpca.9b01992.

35 S. V. Ryazantsev, V. I. Feldman and L. Khriachtchev, Conformational switching of HOCO radical: selective vibrational excitation and hydrogen-atom tunneling, *J. Am. Chem. Soc.*, 2017, **139**(28), 9551–9557, DOI: 10.1021/jacs.7b02605.

36 S. Góbi, I. Reva, I. P. Csonka, M. C. Nunes, G. Tarczay and R. Fausto, Selective conformational control by excitation of NH imino vibrational antennas, *Phys. Chem. Chem. Phys.*, 2019, **21**(45), 24935–24949, DOI: 10.1039/C9CP05370K.

37 R. Fausto and A. Gómez-Zavaglia, Light induced reactions in cryogenic matrices (highlights 2011–2012), in *Photochemistry*, ed. Albini, A. and Fasani, E., The Royal Society of Chemistry, 2013, vol. 41, DOI: 10.1039/9781849737722-00012.

38 R. Fausto, A. Borba and A. Gómez-Zavaglia, Light induced reactions in cryogenic matrices (highlights 2013–2014), in *Photochemistry*, ed. Fasani, E. and Albini, A., The Royal Society of Chemistry, 2015, vol. 43.

39 R. Fausto, T. Nikitin and E. M. Brás, Light induced reactions in cryogenic matrices (highlights 2017–2018), in *Photochemistry*, ed. Albini, A. and Protti, S., The Royal Society of Chemistry, 2019; vol. 47.

40 R. Fausto, T. Nikitin and E. M. Brás, Light induced reactions in cryogenic matrices (2019–2020), in *Photochemistry*, ed. S. Crespi and S. Protti, The Royal Society of Chemistry, 2021, vol. 49.

41 R. Fausto, G. O. Ildiz and C. M. Nunes, IR-induced and tunneling reactions in cryogenic matrices: the (incomplete) story of a successful endeavor, *Chem. Soc. Rev.*, 2022, **51**(7), 2853–2872, DOI: 10.1039/D1CS01026C.

42 M. Freindorf, E. Kraka and D. Cremer, A comprehensive analysis of hydrogen bond interactions based on local vibrational modes, *Int. J. Quantum Chem.*, 2012, **112**(19), 3174–3187, DOI: 10.1002/qua.24118.

43 V. M. Akulin and N. V. Karlov, Redistribution of the vibrational energy in the course of laser excitation of high vibrational levels of polyatomic molecules, *Sov. J. Exp. Theor. Phys.*, 1980, **52**, 1063.

44 V. E. Bondybey, Relaxation and vibrational energy redistribution processes in polyatomic molecules, *Annu. Rev. Phys. Chem.*, 1984, **35**, 591–612, DOI: 10.1146/annurev.pc.35.100184.003111.

45 P. M. Felker and A. H. Zewail, Dynamics of intramolecular vibrational-energy redistribution (IVR). I. Coherence effects, *J. Chem. Phys.*, 1985, **82**(7), 2961–2974, DOI: 10.1063/1.448246.

46 P. M. Felker and A. H. Zewail, Dynamics of intramolecular vibrational-energy redistribution (IVR). II. Excess energy dependence, *J. Chem. Phys.*, 1985, **82**(7), 2975–2993, DOI: 10.1063/1.448247.

47 M. Pettersson, E. M. S. Maçôas, L. Khriachtchev, R. Fausto and M. Räsänen, Conformational isomerization of formic acid by vibrational excitation at energies below the torsional barrier, *J. Am. Chem. Soc.*, 2003, **125**(14), 4058–4059, DOI: 10.1021/ja0295016.

48 L. J. Duarte, C. M. Nunes, R. Fausto and A. A. C. Braga, A protocol for the investigation of the intramolecular vibrational energy redistribution problem: the isomerization of nitrous acid as a case of study, *Phys. Chem. Chem. Phys.*, 2025, **27**(7), 3685–3700, DOI: 10.1039/D4CP04130E.

49 N. Akai, S. Kudoh and M. Nakata, Photoisomerization and tunneling isomerization of tetrachlorohydroquinone in a low-temperature argon matrix, *J. Phys. Chem. A*, 2003, **107**(19), 3655–3659, DOI: 10.1021/jp0225065.

50 S. Lopes, A. V. Domanskaya, R. Fausto, M. Räsänen and L. Khriachtchev, Formic and acetic acids in a nitrogen matrix: enhanced stability of the higher-energy conformer, *J. Chem. Phys.*, 2010, **133**(14), 144507, DOI: 10.1063/1.3484943.

51 J. Krupa, M. Wierzejewska and J. Lundell, Matrix isolation FTIR and theoretical study of weakly bound complexes of isocyanic acid with nitrogen, *Molecules*, 2022, **27**(2), 495, DOI: 10.3390/molecules27020495.

52 J. P. L. Roque, C. M. Nunes, P. R. Schreiner and R. Fausto, Hydrogen tunneling exhibiting unexpectedly small primary kinetic isotope effects, *Chem. – Eur. J.*, 2024, **30**(39), e202401323, DOI: 10.1002/chem.202401323.

53 A. J. Lopes Jesus, R. Fausto and I. Reva, Conformational space, IR-induced, and UV-induced chemistry of carvacrol isolated in a low-temperature argon matrix, *J. Phys. Chem. A*, 2021, **125**(37), 8215–8229, DOI: 10.1021/acs.jpca.1c05907.

54 A. J. Lopes Jesus, C. M. Nunes and I. Reva, Conformational structure, infrared spectra and light-induced transformations of thymol isolated in noble gas cryomatrices, *Photochem*, 2022, **2**(2), 405–422, DOI: 10.3390/photochem2020028.

55 N. Akai, S. Kudoh, M. Takayanagi and M. Nakata, *cis–trans* isomerization equilibrium in hydroquinone in low-temperature argon and xenon matrices studied by FTIR spectroscopy, *Chem. Phys. Lett.*, 2002, **356**(1–2), 133–139, DOI: 10.1016/S0009-2614(02)00379-2.

56 M. M. Quesada-Moreno, A. Krin and M. Schnell, Analysis of thyme essential oils using gas-phase broadband rotational spectroscopy, *Phys. Chem. Chem. Phys.*, 2019, **21**, 26569–26579, DOI: 10.1039/c9cp05583e.

57 D. Schmitz, V. A. Shubert, B. M. Giuliano and M. Schnell, The broadband microwave spectra of the monoterpenoids thymol and carvacrol: conformational landscape and internal dynamics, *J. Chem. Phys.*, 2014, **141**(3), 034304, DOI: 10.1063/1.4887337.

58 P. Pinillos, F. Torres-Hernández, I. Usabiaga, P. Pinacho and J. A. Fernández, Exploration of carvacrol aggregation by laser spectroscopy, *Phys. Chem. Chem. Phys.*, 2024, **26**(37), 24533–24541, DOI: 10.1039/D4CP02945C.

59 A. D. Becke, Density-functional thermochemistry. III. The role of exact exchange, *J. Chem. Phys.*, 1993, **98**(7), 5648–5652, DOI: 10.1063/1.464913.

60 Q. Wu and W. Yang, Empirical correction to density functional theory for van der Waals interactions, *J. Chem. Phys.*, 2002, **116**(2), 515–524, DOI: 10.1063/1.1424928.

61 S. H. Vosko, L. Wilk and M. Nusair, Accurate spin-dependent electron liquid correlation energies for local spin density calculations: a critical analysis, *Can. J. Phys.*, 1980, 1200–1211.

62 P. J. Stephens, F. J. Devlin, C. F. Chabalowski and M. J. Frisch, *Ab initio* calculation of vibrational absorption and circular dichroism spectra using density functional force fields, *J. Phys. Chem.*, 1994, **98**(45), 11623–11627, DOI: 10.1021/j100096a001.

63 V. Barone, Anharmonic vibrational properties by a fully automated second-order perturbative approach, *J. Chem. Phys.*, 2005, **122**(1), 014108, DOI: 10.1063/1.1824881.

64 V. Barone, J. Bloino, C. A. Guido and F. Lipparini, A fully automated implementation of VPT2 infrared intensities, *Chem. Phys. Lett.*, 2010, **496**(1–3), 157–161, DOI: 10.1016/j.cplett.2010.07.012.

65 V. Barone, M. Biczysko and J. Bloino, Fully anharmonic IR and Raman spectra of medium-size molecular systems: accuracy and interpretation, *Phys. Chem. Chem. Phys.*, 2014, **16**(5), 1759–1787, DOI: 10.1039/C3CP53413H.

66 M. J. Frisch, G. W. Trucks, H. B. Schlegel, G. E. Scuseria, M. A. Robb, J. R. Cheeseman, G. Scalmani, V. Barone, G. A. Petersson, H. Nakatsuji, X. Li, M. Caricato, A. V. Marenich, J. Bloino, B. G. Janesko, R. Gomperts, B. Mennucci, H. P. Hratchian, J. V. Ortiz, A. F. Izmaylov, J. L. Sonnenberg, D. Williams-Young, F. Ding, F. Lipparini, F. Egidi, J. Goings, B. Peng, A. Petrone, T. Henderson, D. Ranasinghe, V. G. Zakrzewski, J. Gao, N. Rega, G. Zheng, W. Liang, M. Hada, M. Ehara, K. Toyota, R. Fukuda, J. Hasegawa, M. Ishida, T. Nakajima, Y. Honda, O. Kitao, H. Nakai, T. Vreven, K. Throssell, J. A. Montgomery, Jr., J. E. Peralta, F. Ogliaro, M. J. Bearpark, J. J. Heyd, E. N. Brothers, K. N. Kudin, V. N. Staroverov, T. A. Keith, R. Kobayashi, J. Normand, K. Raghavachari, A. P. Rendell, J. C. Burant, S. S. Iyengar, J. Tomasi, M. Cossi, J. M. Millam, M. Klene, C. Adamo, R. Cammi, J. W. Ochterski, R. L. Martin, K. Morokuma, O. Farkas, J. B. Foresman and D. J. Fox, *Gaussian 16 Revision C.01*, 2016.

67 D. Schmitz, V. A. Shubert, B. M. Giuliano and M. Schnell, The broadband microwave spectra of the monoterpenoids thymol and carvacrol: conformational landscape and internal dynamics, *J. Chem. Phys.*, 2014, **141**(3), 034304, DOI: 10.1063/1.4887337.